tracer binding in the parietal areas was modest. The pattern of tracer distribution correlated with the known distribution of tau pathology (Fig. 6A), but not with the known distribution of Aβ nor the binding of [^{11}C]PiB (data not shown). In addition, quantitative analyses of these images demonstrated significant correlation of ^{18}F-THK-5105 binding with tau immunostained areas, but not with the areas of Aβ immunostaining (Fig. 6B, Fig. S3). In contrast, [^{11}C]PiB bindings showed good correlation with Aβ deposition, but not with tau deposition (Fig. S3).

Pharmacokinetics in Mice

All tested compounds exhibited sufficient amounts of tracer uptake in the mouse brain immediately after intravenous administration. Compared with ^{18}F-THK-523, new THK compounds showed significantly higher brain uptake at 2 min p.i. (Table 2). ^{18}F-THK-5105 showed the highest brain uptake. In addition, clearance of these derivatives from normal brain tissue was faster than that of ^{18}F-THK-523 and ^{18}F-FDDNP (Table 2). The brain uptake ratio at 2 min versus 60 min was highest for ^{18}F-THK-5117, followed by ^{18}F-THK-5105, ^{18}F-THK-5116, ^{18}F-FDDNP, and ^{18}F-THK-523. After injection of ^{18}F-THK-5105 and ^{18}F-THK-5117, the regional tracer uptake in the liver was highest at 10 min p.i., and the tracer was then slowly washed out from the body (Fig. 7). Compared with ^{18}F-THK-5105, ^{18}F-THK-5117 tended to

have faster clearance from the brain, blood, liver, and kidney. No remarkable accumulation of ^{18}F-THK-5105 and ^{18}F-THK-5117 was observed in the bone.

Animal Toxicity Studies

A single intravenous administration of THK-5105 and THK-5117 at 1 mg/kg, equivalent to 100,000-fold the intended clinical dose for humans, caused no systemic toxicity in rats or mice. There were no unscheduled deaths or morbidity detected in this study. During the experimental period, the body weight of all animals increased normally, and no treatment-related changes were noted in any animals. There were no major clinical, biochemical, or histopathological findings associated with the administration of THK-5105 and THK-5117.

Receptor Binding Assays

Binding inhibition of THK-5105 and THK-5117 was assessed in competitive radioligand binding assays against 60 common neurotransmitter receptors, ion channels and transporters. As a result, no remarkable inhibition (<50%) was observed for various receptors, ion channels and transporters at 1 μM concentrations of THK-5105 and THK-5117.

DISCUSSION

These findings suggest that ^{18}F-THK-5105 and ^{18}F-THK-5117 are promising candidates as tau imaging PET probes. Although previous saturation analysis showed the high binding affinity of ^{18}F-THK-523 for tau fibrils (Kd = 1.67 nM), current competition assay demonstrated relatively lower binding affinity of THK-523 for tau fibrils (Ki = 59.3 nM) than THK-5105 (Ki = 7.8 nM) and THK-5117 (Ki = 10.5 nM). ^{18}F-THK-5105 showed higher affinity for tau pathology than for Aβ pathology in AD brain sections. Most amyloid imaging agents potentially bind to both tau and Aβ fibrils, because both protein fibrils share a common β-sheet secondary structure. To ensure the binding specificity of these compounds as tau-selective PET probes, the binding affinity to Aβ fibrils should be below the *in vivo* detection threshold. *In vitro* binding assays indicated that the binding affinity of ^{18}F-THK-5105 for Aβ fibrils (K_d = 35.9 nM) was 25 times lower than to tau fibrils (K_d = 1.45 nM). This K_d would allow selective detection of tau pathology, because the usual required K_d values for imaging Aβ are below 20 nM(*34*). However, the required K_d value for imaging tau deposits is still unknown. Considering that the concentrations of tau are about an order of magnitude lower than those of Aβ, the K_d value for tau should be well below 20 nM, in the low nanomolar range, to allow sensitive detection of tau pathology. In that respect, the binding affinities of both ^{18}F-THK-5105 and ^{18}F-THK-5117 to tau fibrils may be sufficient for *in vivo* detection of tau pathology in the brain. However, *in vitro* binding assay data should be carefully interpreted, because the structural conformation of

synthetic tau fibrils does not fully correlate with the structure of NFTs and neuropil threads in the human brain. Actually, ^{18}F-THK-523 showed substantially lower affinity for AD brain homogenates (Kd = 86.5 nM) than for synthetic tau protein fibrils (Kd = 1.67 nM)(*15*). In the future, *in vitro* binding data should be compared with *in vivo* PET data to determine the required K_d value for *in vivo* tau detection.

In vitro assays using human brain samples are considered more reliable for evaluating the binding selectivity of radiotracers to tau and Aβ pathology at tracer doses. Autoradiography studies using human brain sections demonstrated the preferential binding of ^{18}F-THK-5105 and ^{18}F-THK-5117 to tau protein deposits in AD brain. We observed a high density of ^{18}F-THK-5105 and ^{18}F-THK-5117 binding in the CA1 region of AD hippocampus, which contained substantial amounts of NFTs and neuropil threads. In addition, these tracers clearly visualized the laminar distribution of tau in pri-α layer of the transentorhinal and temporal cortices, that is typically observed in AD brain(*5*). The distribution pattern of THK tracer binding in AD brains was different from that of the Aβ imaging probe PiB and BF-227, which showed diffuse punctate distribution in broad neocortical gray matter and less tracer distribution in the mesial temporal region. These findings strongly suggest that binding properties of ^{18}F-THK-5105 and ^{18}F-THK-5117 are very different from those of currently available Aβ PET probes. Compared to ^{18}F-THK-523(*17*), both ^{18}F-THK-5105 and ^{18}F-THK-5117 showed higher

contrast of tau pathology in autoradiographic images. These findings most likely reflect the increased binding affinity to tau by methylation of the amino group, as indicated by *in vitro* binding assays. Similar findings were previously reported in arylbenzothiazole derivatives (*37*). Compared to ^{18}F-THK-5105, ^{18}F-THK-5117 showed lesser tracer binding in the gray matter containing high density of Aβ plaques, suggesting low binding affinity to Aβ and high selectivity to tau. ^{18}F-THK-5105 tends to show higher signals in the gray matter, and some of the images of ^{18}F-THK-5105 binding showed the patchy pattern as observed for PiB binding. One possible reason for this is the binding of ^{18}F-THK-5105 to tau protein in dystrophic neurites. Another possible reason is binding of ^{18}F-THK-5105 to Aβ fibrils. However, the latter explanation seems unlikely given that ^{18}F-THK-5105 binding, as clearly shown in Figure 6, was correlated with tau, and not Aβ deposits.

In vitro binding assays using AD brain homogenates are generally used to measure the binding affinity of Aβ imaging radiotracers to SPs and/or NFTs and the number of binding sites in real AD pathology(*35*). For most of the useful Aβ imaging radiotracers, the reported K_d or K_i values for neocortical brain samples are below 10 nM(*35, 36*). In this study, the K_d values for high affinity sites of AD mesial temporal homogenates were 2.63 nM for ^{18}F-THK-5105 and 5.19 nM for ^{18}F-THK-5117. These binding affinities were higher than that for ^{18}F-THK-523 and appear to be sufficient for *in vivo* detection of AD pathology in the mesial temporal region at

tracer doses. Furthermore, the B_{max}/K_d ratios of ^{18}F-THK-5105 and ^{18}F-THK-5117 for AD brain homogenates were 136.1 and 65.1 respectively, which fulfills the criteria (B_{max}/K_d ratio > 10) for a good neuroimaging agent(*37*).

Optimization of pharmacokinetics is an important aspect in the development of a PET tracer(*38*). ^{18}F-THK-5105, ^{18}F-THK-5116 and ^{18}F-THK-5117 fulfilled the criteria of appropriate Log P value (LogP = 1–3) for brain entry(*39*). In mice, these tracers showed sufficient brain uptake and rapid washout from normal brain tissue. ^{18}F-THK-5105 and ^{18}F-THK-5117 exhibited high initial brain uptake in normal mice (>6%ID/g at 2 min). These values, which are equivalent to over 100% injected dose index in a 25 g mouse, meet the prerequisites for useful PET imaging agents(*34*). The 2 to 60 min ratio of radioactivity concentrations for ^{18}F-THK-5117 was 23.1, indicating faster washout from normal brain for these compounds than for other currently available ^{18}F-labeled tracers such as FDDNP (2.91), florbetaben (4.83)(*40*), and florbetapir (3.90)(*36*). Compared to ^{18}F-THK-523, ^{18}F-THK-5116 washed out faster from normal brain tissue of mice, indicating that the hydroxylation of the fluoroalkoxy group improves pharmacokinetics in mice. However ^{18}F-THK-5116 is not a suitable compound for clinical application, due to its lower initial brain uptake and binding affinity than the other two THK compounds.

CONCLUSION

^{18}F-THK-5105 and ^{18}F-THK-5117 should be considered as promising candidates for PET tau imaging radiotracers. Future clinical studies will clarify the usefulness of these radiotracers for the early detection of AD tau pathology.

ACKNOWLEDGMENTS

This study was supported by the research fund from GE Healthcare, the Industrial Technology Research Grant Program of the NEDO in Japan (09E51025a), Health and Labor Sciences Research Grants from the Ministry of Health, Labor, and Welfare of Japan, Grant-in-Aid for Scientific Research (B) (23390297) and "Japan Advanced Molecular Imaging Program (J-AMP)" of the Ministry of Education, Culture, Sports, Science and Technology (MEXT), Japan.

REFERENCES

1. Organisation for Economic Co-operation and Development (OECD). Understanding the Brain: The Birth of a Learning Science, OECD Publishing, Paris, 2007.

2. Hardy J, Selkoe DJ. The amyloid hypothesis of Alzheimer's disease: progress and problems on the road to therapeutics. *Science.* 2002;297:353-356.

3. Lichtenberg B, Mandelkow EM, Hagestedt T, Mandelkow E. Structure and elasticity of microtubule-associated protein tau. *Nature.* 1988;334:359-362.

4. Holzer M, Holzapfel HP, Zedlick D, Bruckner MK, Arendt T. Abnormally phosphorylated tau protein in Alzheimer's disease: heterogeneity of individual regional distribution and relationship to clinical severity. *Neuroscience.* 1994;63:499-516.

5. Braak H, Braak E. Neuropathological stageing of Alzheimer-related changes. *Acta Neuropathol (Berlin).* 1991;82:239-259.

6. Bondareff W, Mountjoy CQ, Roth M, Hauser DL. Neurofibrillary degeneration and neuronal loss in Alzheimer's disease. *Neurobiol Aging.* 1989;10:709-715.

7. Bobinski M, Wegiel J, Wisniewski HM, et al. Neurofibrillary pathology--correlation with hippocampal formation atrophy in Alzheimer disease. *Neurobiol Aging.*1996;17:909-919.

8. Guillozet AL, Weintraub S, Mash DC, Mesulam MM. Neurofibrillary tangles, amyloid, and memory in aging and mild cognitive impairment. *Arch Neurol.* 2003;60:729-736.

9. Gomez-Isla T, Price JL, McKeel DW, Jr., Morris JC, Growdon JH, Hyman BT. Profound loss of layer II entorhinal cortex neurons occurs in very mild Alzheimer's disease. *J Neurosci.* 1996;16:4491-4500.

10. Okamura N, Suemoto T, Furumoto S, et al. Quinoline and benzimidazole derivatives: candidate probes for in vivo imaging of tau pathology in Alzheimer's disease. *J Neurosci.* 2005;25:10857-10862.

11. Rojo LE, Alzate-Morales J, Saavedra IN, Davies P, Maccioni RB. Selective interaction of lansoprazole and astemizole with tau polymers: potential new clinical use in diagnosis of Alzheimer's disease. *J Alzheimers Dis.* 2010;19:573-589.

12. Ono M, Hayashi S, Matsumura K, et al. Rhodanine and thiohydantoin derivatives for detecting tau pathology in Alzheimer's brains. *ACS Chem Neurosci.* 2011;2:269-275.

13. Jensen JR, Cisek K, Funk KE, Naphade S, Schafer KN, Kuret J. Research towards tau imaging. *J Alzheimers Dis.* 2011;26 Suppl 3:147-157.

14. Zhang W, Arteaga J, Cashion DK, et al. A highly selective and specific PET tracer for imaging of tau pathologies. *J Alzheimers Dis.* 2012; 31:601-612.

15. Fodero-Tavoletti MT, Okamura N, Furumoto S, et al. ^{18}F-THK523: a novel in vivo tau imaging ligand for Alzheimer's disease. *Brain* 2011;134:1089-1100.

16. Villemagne VL, Furumoto S, Fodero-Tavoletti MT, et al. The challenges of tau imaging. *Future Neurol.* 2012;7:409-421.

17. Harada R, Okamura N, Furumoto S, et al. Comparison of the binding characteristics of [^{18}F]THK-523 and other amyloid imaging tracers to Alzheimer's disease pathology. *Eur J Nucl Med Mol Imaging.* 2012;40:125-132.

18. Small GW, Agdeppa ED, Kepe V, Satyamurthy N, Huang SC, Barrio JR. In vivo brain imaging of tangle burden in humans. *J Mol Neurosci.* 2002;19:323-327.

19. Agdeppa ED, Kepe V, Liu J, et al. Binding characteristics of radiofluorinated 6-dialkylamino-2-naphthylethylidene derivatives as positron emission tomography imaging probes for beta-amyloid plaques in Alzheimer's disease. *J Neurosci.* 2001;21:RC189.

20. Thompson PW, Ye L, Morgenstern JL, et al. Interaction of the amyloid imaging tracer FDDNP with hallmark Alzheimer's disease pathologies. *J Neurochem.* 2009;109:623-630.

21. Tolboom N, Yaqub M, van der Flier WM, et al. Detection of Alzheimer pathology in vivo using both 11C-PIB and 18F-FDDNP PET. *J Nucl Med.* 2009;50:191-197.

22. Shoghi-Jadid K, Small GW, Agdeppa ED, et al. Localization of neurofibrillary tangles and beta-amyloid plaques in the brains of living patients with Alzheimer disease. *Am J Geriatr Psychiatry.* 2002;10:24-35.

23. Naslund J, Haroutunian V, Mohs R, et al. Correlation between elevated levels of amyloid beta-peptide in the brain and cognitive decline. *JAMA* 2000;283:1571-1577.

24. Mukaetova-Ladinska EB, Harrington CR, Roth M, Wischik CM. Biochemical and anatomical redistribution of tau protein in Alzheimer's disease. *Am J Pathol.* 1993;143:565-578.

25. Liu J, Kepe V, Zabjek A, et al. High-yield, automated radiosynthesis of 2-(1-{6-[(2-[^{18}F]fluoroethyl)(methyl)amino]-2-naphthyl}ethylidene)malononitrile ([^{18}F]FDDNP) ready for animal or human administration. *Molecular Imaging and Biology* 2007;9:6-16.

26. Fodero-Tavoletti MT, Mulligan RS, Okamura N, et al. In vitro characterisation of BF227 binding to alpha-synuclein/Lewy bodies. *Eur J Pharmacol.* 2009;617:54-58.

27. Wilson AA, Garcia A, Chestakova A, Kung H, Houle S. A rapid one-step radiosynthesis of the beta-amyloid imaging radiotracer N-methyl-[C-11]2-(4 '-methylaminophenyl)-6-hydroxybenzothiazole ([C-11]-6-OH-BTA-1). *J Label Compd Radiopharm.* 2004;47:679-682.

28. Cheng Y, Prusoff WH. Relationship between the inhibition constant (Ki) and the concentration of inhibitor which causes 50 per cent inhibition (IC50) of an enzymatic reaction. *Biochem Pharmacol.* 1973;22:3099-3108.

29. Okamura N, Suemoto T, Shimadzu H, et al. Styrylbenzoxazole derivatives for in vivo imaging of amyloid plaques in the brain. *J Neurosci.* 2004;24:2535-2541.

30. Ikeda K, Akiyama H, Kondo H, Haga C. A study of dementia with argyrophilic grains. Possible cytoskeletal abnormality in dendrospinal portion of neurons and oligodendroglia. *Acta Neuropathol (Berlin).* 1995;89:409-414.

31. Bouras C, Hof PR, Giannakopoulos P, Michel JP, Morrison JH. Regional distribution of neurofibrillary tangles and senile plaques in the cerebral cortex of elderly patients: a quantitative evaluation of a one-year autopsy population from a geriatric hospital. *Cereb Cortex.*1994;4:138-150.

32. Kudo Y, Okamura N, Furumoto S, et al. 2-(2-[2-Dimethylaminothiazol-5-yl]ethenyl)-6- (2-[fluoro]ethoxy)benzoxazole: a novel PET agent for in vivo detection of dense amyloid plaques in Alzheimer's disease patients. *J Nucl Med.* 2007;48:553-561.

33. Braak H, Alafuzoff I, Arzberger T, Kretzschmar H, Del Tredici K. Staging of Alzheimer disease-associated neurofibrillary pathology using paraffin sections and immunocytochemistry. *Acta Neuropathol (Berlin).* Oct 2006;112(4):389-404.

34. Mathis CA, Wang Y, Klunk WE. Imaging beta-amyloid plaques and neurofibrillary tangles in the aging human brain. *Curr Pharm Des.* 2004;10:1469-1492.

35. Klunk WE, Wang Y, Huang GF, et al. The binding of 2-(4'-methylaminophenyl)benzothiazole to postmortem brain homogenates is dominated by the amyloid component. *J Neurosci.* 2003;23:2086-2092.

36. Choi SR, Golding G, Zhuang Z, et al. Preclinical properties of 18F-AV-45: a PET agent for Abeta plaques in the brain. *J Nucl Med.* 2009;50:1887-1894.

37. Mathis CA, Wang Y, Holt DP, Huang GF, Debnath ML, Klunk WE. Synthesis and evaluation of 11C-labeled 6-substituted 2-arylbenzothiazoles as amyloid imaging agents. *J Med Chem.* 2003;46:2740-2754.

38. Furumoto S, Okamura N, Iwata R, Yanai K, Arai H, Kudo Y. Recent advances in the development of amyloid imaging agents. *Curr Top Med Chem.* 2007;7:1773-1789.

39. Waterhouse RN. Determination of lipophilicity and its use as a predictor of blood-brain barrier penetration of molecular imaging agents. *Molecular Imaging and Biology* 2003;5:376-389.

40. Zhang W, Oya S, Kung MP, Hou C, Maier DL, Kung HF. F-18 Polyethyleneglycol stilbenes as PET imaging agents targeting Abeta aggregates in the brain. *Nucl Med Biol.* 2005;32:799-809.

FIGURE LEGENDS:

Figure 1: Chemical structures of ^{18}F-THK-5105, ^{18}F-THK-5116, ^{18}F-THK-5117, and ^{18}F-THK-523

Figure 2: Radiosynthesis scheme of ^{18}F-2-arylquinolines

Figure 3: Competitive inhibition of ^{18}F-THK-5105 binding by 2-arylquinolines and FDDNP to tau protein fibrils. The Ki value for inhibition of ^{18}F-THK-5105 binding to tau are shown.

Figure 4: Neuropathological staining of brain sections from Alzheimer's disease (AD) patients. Neurofibrillary tangles and neuropil threads were clearly stained with THK-5105 (**A, C**). These stainings were consistent with tau immunostaining (**B**) and Gallyas-Braak staining (**D**) in the same sections. Bar = 50 μm

Figure 5: (**A**) Autoradiographic images of ^{18}F-THK-5105 (left), ^{18}F-THK-5117 (center) and [^{11}C]PiB (right) binding in mesial temporal section from the AD patient. (**B**) Gallyas-Braak silver staining (left) and the immunostaining with anti-tau (center) and anti-Aβ (right) antibodies in adjacent brain sections.

Figure 6: Autoradiography of hemibrain sections from the AD patient with ^{18}F-THK-5105 (**A**) and tau immunostaining (**B**) in the neighboring section. The region of interest analysis (**D**) indicated that % areas of ^{18}F-THK-5105 binding (line plots) were significantly correlated with % areas of tau immunostaining (gray bars), but not with that of Aβ immunostaining (white bars).

HIP: hippocampus, PHG: parahippocampal gyrus, FUG: fusiform gyrus, ITG: inferior temporal gyrus, MTG: middle temporal gyrus, STG: superior temporal gyrus, INS: insula, POG: postcentral gyrus, PRG: precentral gyrus, SFG: superior frontal gyrus, PCL: paracentral lobule, CG: cingulate gyrus

Figure 7: Time activity curves after intravenous administration of ^{18}F-THK-5105 (**A**) and ^{18}F-THK-5117 (**B**) in mice

Supplementary data

Figure S1: Saturation binding curves and Scatchard plots of ^{18}F-THK-5105 and ^{18}F-THK-5117 for mesial temporal brain homogenates of AD patient

Figure S2: Autoradiographic images of ^{18}F-THK-5105 (**A**) and ^{18}F-THK-5117 (**B**) in mesial temporal brain sections of healthy control subject (62-year-old man)

Figure S3: (**A**) Correlational analysis of % areas of ^{18}F-THK-5105 binding with % areas of tau (left) and Aβ (right) immunostaining. (**B**) Correlational analysis of % areas of [^{11}C]PiB binding with % areas of tau (left) and Aβ (right) immunostaining.

Table 1: K_D and B_{max} values of ^{18}F-THK-5105 for synthetic tau and $A\beta_{1-42}$ fibrils

	K_{D1}	B_{max1}	K_{D2}	B_{max2}
Tau	1.45	6.89	7.40	20.05
$A\beta_{1-42}$	35.9	61.6		

K_D are in nM and Bmax are in pmol ^{18}F-THK-5105/nmol fibrils.

Table 2: Log P and brain uptakes after intravenous administration of ^{18}F-labeled compounds in mice

	Log P	Brain uptakes (%ID/g)			Brain uptake ratio (2 min / 60 min)
		2 min p.i.	30 min p.i.	60 min p.i.	
^{18}F-THK-523	2.40	2.72	1.47	1.46	1.86
^{18}F-THK-5105	3.03	9.20	3.61	1.00	9.20
^{18}F-THK-5116	1.57	3.36	0.75	0.57	5.89
^{18}F-THK-5117	2.32	6.06	0.59	0.26	23.1
^{18}F-FDDNP	3.71	6.23	2.02	2.14	2.91

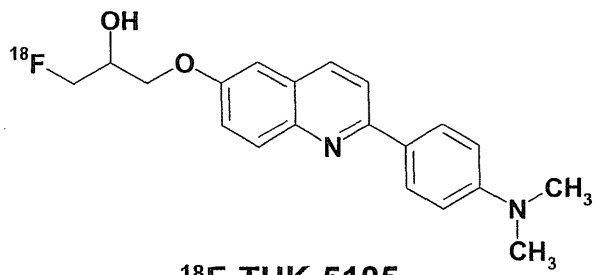

^{18}F-THK-5105

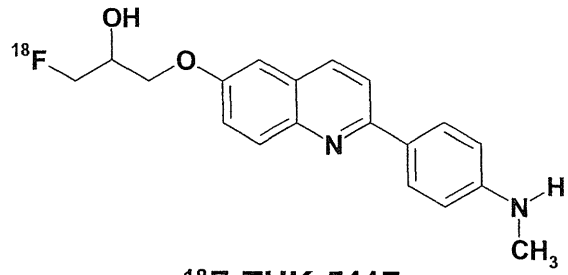

^{18}F-THK-5117

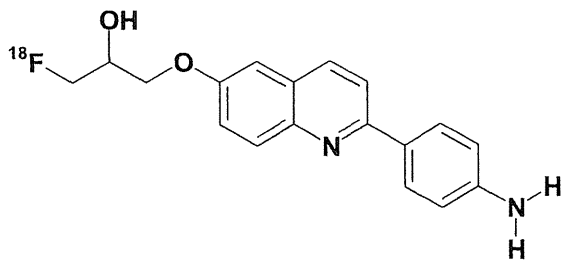

^{18}F-THK-5116

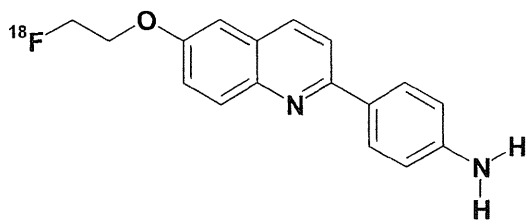

^{18}F-THK-523

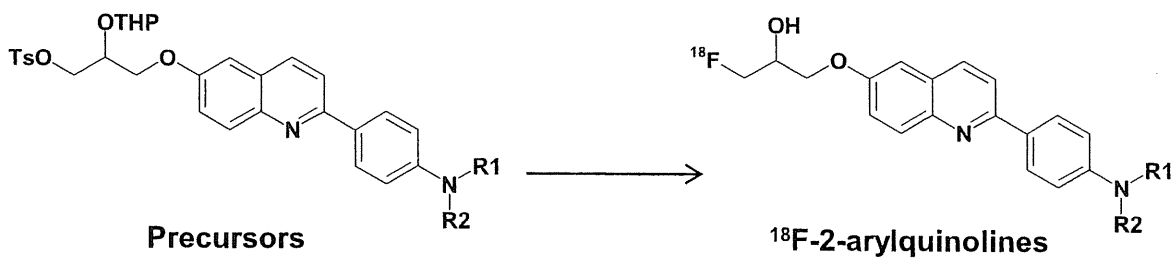

THK-5105, R1 = R2 = CH_3
THK-5116, R1 = R2 = H
THK-5117, R1 = H, R2 = CH_3

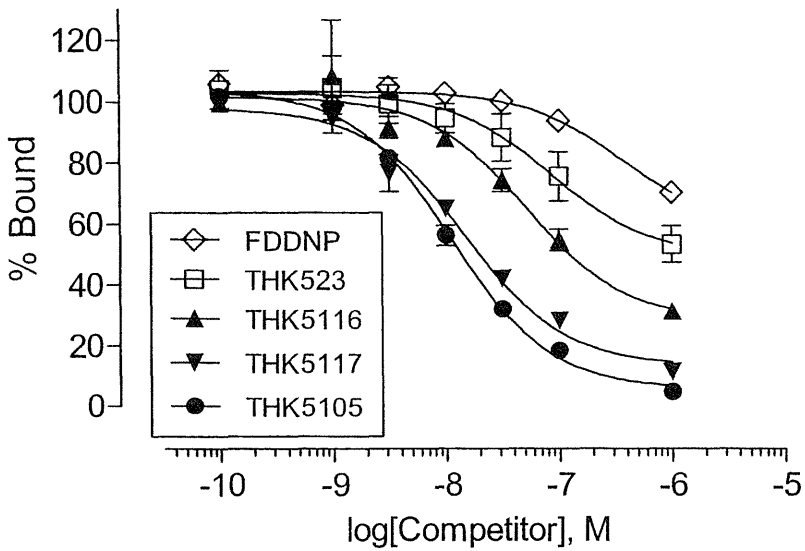

Compounds	Ki (nM)
THK-5105	7.8
THK-5116	36.0
THK-5117	10.5
THK-523	59.3
FDDNP	263